

# Efficient calculation of time-optimal motion primitives for systems exhibiting oscillatory internal dynamics with multiple applications.

1<sup>st</sup> Thomas Auer  
IACE - UMIT TIROL  
Hall in Tirol, Austria  
thomas.auer@umit-tirol.at

2<sup>nd</sup> Frank Woittennek  
IACE - UMIT TIROL  
Hall in Tirol, Austria  
frank.woittennek@umit-tirol.at

*Abstract*—A fast algorithm for planning near time-optimal trajectories for systems with an oscillatory internal dynamics has been developed in previous work. In this algorithm, trajectories are assembled from special motion primitives called jerk segments, which are connected by segments of constant acceleration and velocity respectively. It was shown, that the algorithm achieves a time advantage over established trajectory planning methods. Achieving the fastest transition possible with this algorithm may require a redesign of the jerk segments within the motion planning procedure. This publication presents an efficient numerical algorithm enabling for the fast real-time computation of these segments. This is achieved by explicitly evaluating the optimality conditions arising from the maximum principle for input-constrained systems, and further by reducing the evaluation of these conditions to a line-search problem on a bounded interval. This reduction guarantees, that a valid solution is found within a predictable time. Furthermore, the algorithm further does not rely on complicated optimisation algorithms, which allows it to be implemented on low-power hardware.

*Note to Practitioners*—This publication focuses on trajectory planning for systems where oscillation at the end of the motion must be avoided. An example of such systems are high-precision pick-and-place systems in the semiconductor industry. The focus of this publication is put on the calculation of motion profiles that can be easily assembled into complete trajectories, planned in such a way that each provides an oscillation-free transition between different acceleration levels. By combining several such segments, complete trajectories can be calculated. A supplementary publication shows the calculations required for a one-dimensional pick-and-place system, but trajectory planning in multi-dimensional configuration spaces is possible as well. The main advantage of the calculation presented here lies in its ease of implementation, where a time-optimal solution for the motion profiles is calculated without the need for sophisticated optimisation algorithms. Furthermore, the calculation does not rely on specialised mathematical libraries, allowing implementation even on low-power industrial controllers.

*Index Terms*—Motion-planning, Optimization methods, Motion Control

This work has been submitted to the IEEE for possible publication. Copyright may be transferred without notice, after which this version may no longer be accessible.

## I. INTRODUCTION

Pick-and-place processes in the electronics industry require high accuracy and speed. Current developments in further integration and miniaturisation require high accuracy in component placement [18]. High accuracy is required for proper component placement to ensure electrical connections work as intended. To reduce cost, short transitions are desirable. Motion forces on the machine frame combined with finite stiffness lead to oscillation and inaccuracy in component placement. The oscillation of the machine frame can be greater than the accuracy requirements, which are in the  $\mu\text{m}$  range [1]. Specially planned motion profiles, also called trajectories, are used to achieve transitions between different equilibria [4], [5].

In general, trajectory shapers can be used to remove oscillations from systems. A commonly used trajectory shaper (often called a trajectory filter) is the ZV-filter [28], which relies on knowledge of the system dynamics and parameters. Parameter uncertainty due to operational loads [33] or model uncertainty from linear approximation [19] lead to residual oscillations at the end of the transition [4]. Shapers specifically optimised for parameter insensitivity exist and are well studied [21], [14], [13], [27], [24], [26], [31]. Insensitivity to parameter changes is usually associated with longer shaper durations and thus slower movements. So-called negative impulse shapers can be used to shorten the transition times. Special care must be taken to properly account for the kinematic constraints of the actuators [29], [30]. It has been found by [8] that negative impulse shapers can lead to a reduction in transition time, while providing less sensitivity to ZV-filters for selected regions of parameter uncertainty. Other approaches focus on adjusting the jerk to avoid oscillations altogether without using a filter [20], [15]. This publication presents an optimisation-based approach aimed at reducing transition times that is easy to implement and does not rely on complicated optimization libraries.

### A. Contribution of this paper

Unlike algorithms such as [11], [22], [7], [6], [32], which can be used to plan trajectories, the approach presented in this paper considers not only the state variables of the

actuated joints, but also the kinematic state variables of the free oscillation of the system. Compared to ZV-filters, a reduction of the transition time can be achieved. The method is based on the assembly of trajectories from pre-planned jerk profiles (also called motion primitives). The method of trajectory assembly is presented in [3], where the potential for improvement in terms of transition time is highlighted. This publication focuses on the efficient method of calculating the jerk profiles themselves. This publication solves the problem mentioned by [9] by considering the efficient calculation of the jerk segments. It should be noted that although the efficient calculation of the jerk segments is primarily intended for use in the algorithm presented in [3], there are other possible uses for the jerk segments (see Section V). This paper presents the algorithm used to compute these motion profiles in an efficient way that does not rely on complicated optimisation libraries. This should allow the numerical algorithms to be directly evaluated on a low power industrial controller.

### B. Organisation of paper

This paper is organized into the following chapters. The system model is introduced in Section II. The method of assembling the trajectories from jerk segments is sketched very briefly in Section III. The efficient method of calculating the individual jerk segments for the full trajectories is in Section IV. The results are then summarized in Section V and an outlook for relevant follow-up research is given.

The majority of the plots in the contribution were created with the parameters given in Table I in Section II. In order to show certain effects in the algorithm, some parts of the calculation required a different set of parameters. Whenever different parameters are used, it is marked in the plots accordingly and the parameters are given. To be as non-specific to a parameter-set as possible, normalization steps are included in order to simplify and generalize the calculation.

## II. MODEL AND MATHEMATICAL BACKGROUND

As mentioned in [3], the pick-and-place machine is modelled as a lumped system with two masses (mass of the baseframe  $m_b$  and mass of the slider  $m_s$ ), a spring with stiffness  $k$  and a viscous damping element with damping parameter  $d$ . The schematic representation of the system is shown in Figure 1. This was chosen over a continuum-

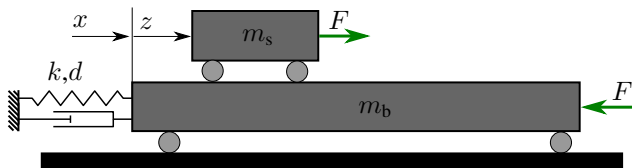


Fig. 1: Symbolic representation of one axis of the pick-and-place machine.

mechanics description, which it was deemed sufficient [16], [5], because the essential oscillation of the machine frame

can be captured by the first mode of the flexible system. Momentum balance allows to derive the equations of motion

$$m_b \ddot{x}(t) + d \dot{x}(t) + k x(t) = -F(t), \quad (1a)$$

$$m_s (\ddot{x}(t) + \ddot{z}(t)) = F(t). \quad (1b)$$

and the parameters used in the numerical studies are listed in Table I. The kinematic constraints listed in Table II correspond

TABLE I: Parameters and resulting eigenfrequencies

$m_s = 25 \text{ kg}$	$m_b = 500 \text{ kg}$	$k = 15 \cdot 10^6 \text{ N/m}$	$d = 5 \cdot 10^3 \text{ kg/s}$
$f_0 = 26.9 \text{ Hz}$		$f_d = 26.8914 \text{ Hz}$	

to an exemplary production machine. It is advantageous to use

TABLE II: Kinematic constraints of slider.

$ \dot{z}(t)  \leq v_{\text{lim}}$	$ \ddot{z}(t)  \leq a_{\text{lim}}$	$ z^{(3)}(t)  \leq j_{\text{lim}}$
$v_{\text{lim}} = 1.5 \text{ m/s}$	$a_{\text{lim}} = 20 \text{ m/s}^2$	$j_{\text{lim}} = 800 \text{ m/s}^3$

a dynamic extension [3] with  $z^{(3)}(t)$  as input for the calculations required later on. Adding (1a) and (1b) together to remove  $F(t)$ , using  $m_g = m_s + m_b$  and selecting  $u(t) = z^{(3)}(t)$  as the input of the dynamic extension leads to the state-space representation

$$\dot{\mathbf{x}} = \underbrace{\begin{bmatrix} 0 & 1 & 0 & 0 & 0 \\ -k^* & -d^* & 0 & 0 & -m^* \\ 0 & 0 & 0 & 1 & 0 \\ 0 & 0 & 0 & 0 & 1 \\ 0 & 0 & 0 & 0 & 0 \end{bmatrix}}_A \cdot \begin{bmatrix} x \\ \dot{x} \\ z \\ \dot{z} \\ \ddot{z} \end{bmatrix} + \underbrace{\begin{bmatrix} 0 \\ 0 \\ 0 \\ 0 \\ 1 \end{bmatrix}}_b z^{(3)}$$

$k^* = k/m_g \quad d^* = d/m_g \quad m^* = m_s/m_g$

with the state and input

$$\mathbf{x} = [x, \dot{x}, z, \dot{z}, \ddot{z}]^T, \quad u = z^{(3)}. \quad (2)$$

## III. METHOD EXPLAINED: OCP-J

This section gives an overview over OCP-J and shows how it can be used to calculate trajectories. Since this is the major content of [3], this section is kept brief and only serves as an introduction to show, how the results of this publication can be used. The essential idea is, that a complete trajectory is assembled from individual motion primitives (called jerk segments), as shown in Figure 2. In order to ensure transitions

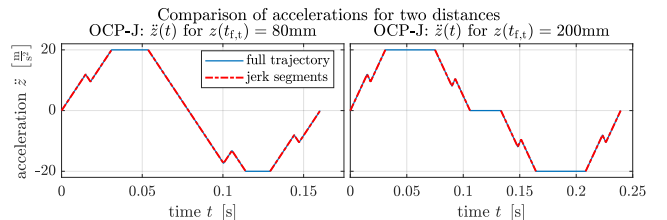


Fig. 2: Two OCP-J trajectories demonstrating how a full trajectory is assembled from the jerk segments (picture taken from [3]).

in minimal time, those jerk segments themselves have to be

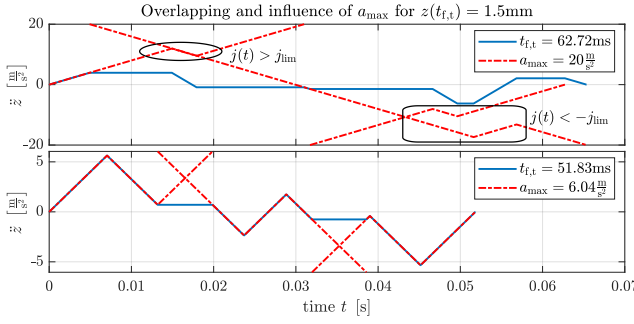


Fig. 3: Showing the overlapping without adjustment of  $a_{\max}$  for a transition distance of  $z(t_{f,t}) = 1.5\text{mm}$  to show the advantage of recalculation of jerk segments in order to reduce the transition time. Picture taken from [3].

time-optimal transitions as shown in [3]. The reason, why fast calculation is required is shown in Figure 3. The comparison with the trajectory with adjusted  $a_{\max}$  shows, that the lower acceleration limit of  $a_{\max} = 6.04\text{ m/s}^2$  removes the violation of the jerk constraint and also leads to a faster transition (for this specific distance). As the analysis of the different trajectory cases [3] showed, fast recalculation of the jerk segments is vital to ensure quick calculation of the overall trajectory. The algorithm to calculate the jerk segments efficiently is presented in Section IV.

#### IV. EFFICIENT ALGORITHM TO CALCULATE THE JERK SEGMENTS

As demonstrated in [3] and shown in Figure 3, recalculation of the jerk segments is required to ensure minimal transition times  $t_{f,t}$ . The algorithm to ensure this, is the main part of this section (and this contribution as well). The jerk segments can be obtained as the solution of an optimization problem with cost

$$\min_{\mathbf{x} \in \mathbb{R}^n, u \in [-j_{\max}, j_{\max}]} J(\mathbf{x}(t), \mathbf{u}(t), t), \quad (3a)$$

$$J(\mathbf{x}(t), \mathbf{u}(t), t) = \int_0^{t_f} 1 dt = t_f. \quad (3b)$$

At the end of the segment  $t_f$ , a certain acceleration (called  $a_{\max}$ ) should be reached, while the oscillation of the base  $x(t)$  has to be equal to zero. The acceleration  $\ddot{z}(t)$  of the slider is constant at this point, resulting in a constant displacement of the base  $x(t)$ . Since the model and parameters are known, this results in a transition of the system state variables (2) from

$$\mathbf{x}(0) = [x, \dot{x}, z, \dot{z}, \ddot{z}]^T = [0, 0, 0, 0, 0]^T \quad (4)$$

to the partly constraint end state (rest of system state variables are left open)

$$\mathbf{x}(t_f) = [x, \dot{x}, \ddot{z}]^T = \left[ -\frac{a_{\max} m_s}{k}, 0, a_{\max} \right]^T. \quad (5)$$

Twice continuously differentiable trajectories  $t \mapsto z(t)$ , which are piecewise constant in  $z^{(3)}(t)$  are considered, since

they allow to limit the velocity, acceleration and the jerk. Those equations allow to use Pontryagin's Maximum Principle (PMP) [23] to solve the problem time-optimally and show the necessary optimality conditions.

#### A. Optimality conditions

In the following, Pontryagin's maximum principle [23] is employed in order to solve the optimization problem (3). With the co-state (or adjoint state)  $\boldsymbol{\lambda}(t) = (\lambda_1(t), \dots, \lambda_5(t))^T$  the Hamiltonian [23], [2], [12] required to formulate the optimality conditions is given by

$$H(\boldsymbol{\lambda}, \mathbf{x}, u) = 1 + \boldsymbol{\lambda}^T (\mathbf{A}\mathbf{x} + \mathbf{b}u) = u\lambda_5 + \mathcal{R}(\mathbf{x}, \boldsymbol{\lambda})$$

with

$$\mathcal{R}(\mathbf{x}, \boldsymbol{\lambda}) = \lambda_1 \dot{x} + \lambda_2 (-k^*x - d^*\dot{x} - m^*\ddot{z}) + \lambda_3 \dot{z} + \lambda_4 \ddot{z}.$$

According to the maximum principle  $u(t)$  must satisfy<sup>1</sup>

$$\begin{aligned} u(t) &= \arg \min_{\bar{u} \in [-j_{\max}, j_{\max}]} H(\mathbf{x}(t), \boldsymbol{\lambda}(t), \bar{u}) \\ &= \arg \min_{\bar{u} \in [-j_{\max}, j_{\max}]} \lambda_5(t) \bar{u} + \mathcal{R}(\mathbf{x}(t), \boldsymbol{\lambda}(t)). \end{aligned}$$

Hence,

$$u(t) = \begin{cases} -j_{\max}, & \text{if } \lambda_5(t) > 0, \\ j_{\max}, & \text{if } \lambda_5(t) < 0. \end{cases} \quad (6)$$

Therefore, the time-optimal control law corresponds to a bang-bang behaviour. Further (necessary) optimality conditions are constituted by the adjoint equations

$$\dot{\lambda}_i = -\frac{\partial H}{\partial x_i}, \quad i = 1, \dots, 5,$$

i.e.,

$$\dot{\lambda}_1 = \lambda_2 k^*, \quad (7a)$$

$$\dot{\lambda}_2 = \lambda_2 d^* - \lambda_1, \quad (7b)$$

$$\dot{\lambda}_3 = 0, \quad (7c)$$

$$\dot{\lambda}_4 = -\lambda_3, \quad (7d)$$

$$\dot{\lambda}_5 = \lambda_2 m^* - \lambda_4. \quad (7e)$$

Finally, initial and terminal conditions for the state variables in  $\mathbf{x}(t)$  as well as the transversality conditions associated with the unconstrained final values of the third and fourth system state variable ( $z(t_f), \dot{z}(t_f)$ ) read<sup>2</sup>

$$x(0) = 0, \quad x(t_f) = -\frac{a_{\max} m_s}{k}, \quad (8a)$$

$$\dot{x}(0) = 0, \quad \dot{x}(t_f) = 0, \quad (8b)$$

$$z(0) = 0, \quad \lambda_3(t_f) = 0, \quad (8c)$$

$$\dot{z}(0) = 0, \quad \lambda_4(t_f) = 0, \quad (8d)$$

$$\ddot{z}(0) = 0, \quad \ddot{z}(t_f) = a_{\max}. \quad (8e)$$

<sup>1</sup>For convenience we do not explicitly distinguish the time optimal trajectory.

<sup>2</sup>Note that the optimal control problem can be equivalently posed on  $\mathbb{R}^3$  with state  $(x(t), \dot{x}(t), \ddot{z}(t))^T$ . However, for the sake of readability the full state is retained here, which does not increase complexity.

Therein, the constraints on the final state result from  $\dot{x}(t_f) = \ddot{x}(t_f) = 0$ , which correspond to an equilibrium of the oscillatory internal dynamics, while taking into account the terminal constraint on  $\ddot{z}$ , i.e.,  $\ddot{z}(t_f) = a_{\max}$ . The adjoint equations (7c) and (7d) in connection the transversality conditions (8c) and (8d) result in

$$\lambda_3(t) = \lambda_4(t) = 0. \quad (9)$$

In order to calculate the required input in accordance with (6), an equivalent second order differential equation for  $\lambda_2$  is deduced from (7a) and (7b):

$$\ddot{\lambda}_2(t) = d^* \dot{\lambda}_2(t) - k^* \lambda_2(t).$$

Using  $\delta = d^*/2$ ,  $\omega_0^2 = k^*$  and  $\omega_d^2 = k^* - \delta^2$  the general solution of this equation is

$$\lambda_2(t) = A_2 e^{\delta t} \cos(B_2 + \omega_d t). \quad (10)$$

Moreover, in view of (9) and (7e),  $\lambda_5$  is obtained by integrating (10):

$$\lambda_5(t) = A_2 \frac{m_s}{k} e^{\delta t} [\delta \cos(B_2 + \omega_d t) + \omega_d \sin(B_2 + \omega_d t)] + C_2.$$

This expression is rewritten with appropriate constants:

$$\lambda_5(t) = A_1 e^{\delta t} \sin(B_1 + \omega_d t) + C_2.$$

Since the problem exhibits free end time, taking the end conditions (8) into account, an additional transversality condition is given by

$$\begin{aligned} 0 &= H(\mathbf{x}(t_f), \boldsymbol{\lambda}(t_f), u(t_f)) \\ &= \lambda_5(t_f) \dot{j}_{\max} + 1 - \lambda_2(t_f) m^* a_{\max}. \end{aligned}$$

In the generic case,

$$(\delta - k^* a_{\max}) \cos(B_2 + \omega_d t_f) + \omega_d \sin(B_2 + \omega_d t_f) \neq 0,$$

the transversality condition can always be met by appropriately choosing  $A_2$ , which in turn determines  $A_1$ . Otherwise,

$$C_2 = -\frac{1}{\dot{j}_{\max}}.$$

In the following, only the generic case is considered. For convenience

$$\lambda_5(t) = A_1 \cdot e^{-\delta \frac{B_1}{\omega_d}} \lambda_{5,n}(t)$$

is reformulated with the normalized quantity

$$\lambda_{5,n} \left( t - \frac{B_1}{\omega_d} \right) = e^{\delta t} \sin(\omega_d t) - C_1. \quad (12)$$

In view of (6) it remains to compute the switching points  $t_i \in [0, t_f]$ ,  $i = \{2, \dots, n-1\}$ , i.e., the zeros of  $\lambda_{5,n}(t)$ . Note that the Theorem on  $n$ -intervals [10] does not apply here, since the system has conjugate complex poles. Therefore, the number of switching points is not a priori fixed. However, an upper bound  $\hat{t}_f = \frac{a_{\max}}{\dot{j}_{\max}} + \frac{\pi}{\omega_d}$  for  $t_f$  results from the application of a ZV-shaper [25], [28], which satisfies all constraints of the posed optimal control problem while not being a time-optimal transition. As a consequence, independently of the constant  $C_1$

and the damping  $\delta$ , the number of switching points is bounded from above. As a consequence, the following result holds:

*Theorem 1:* The optimal control problem (3) possesses a solution  $(\mathbf{x}, u, t_f)$ , satisfying the following properties

$$t_f \in \left[ \frac{a_{\max}}{\dot{j}_{\max}}, \frac{a_{\max}}{\dot{j}_{\max}} + \frac{\pi}{\omega_d} \right) \quad (13a)$$

$$u(t) = \sum_{i=1}^{n-1} (-1)^{i+\nu} (H(t-t_i) - H(t-t_{i+1})) \dot{j}_{\max}, \quad t_n = t_f \quad (13b)$$

$$0 \leq n-2 \leq \left\lceil \left[ \frac{a_{\max}}{\dot{j}_{\max}} \frac{\omega_d}{2\pi} + \frac{1}{2} \right] \right\rceil. \quad (13c)$$

Moreover, with (12), the switching points  $t_2, \dots, t_{n-1}$  correspond to the zeros of  $\lambda_{5,n}(t)$ , and

$$\nu = \begin{cases} 0, & \text{if } \lambda_{5,n}(0) > 0, \\ 1, & \text{if } \lambda_{5,n}(0) < 0. \end{cases}$$

Finally, the analytical solutions for the system state variables to such an input are given according to Appendix A and Appendix B.

Two exemplary solutions for  $\lambda_{5,n}(t)$  giving rise to exactly two switchings at  $t_2$  and  $t_3$  are depicted in Figure 4. The parameters are chosen according to Table II. Up to now the optimal control problem considered has been reduced to the computation of the remaining variables  $C_1$ ,  $B_1$  and  $t_f$ , determining the shape of  $\lambda_{5,n}(t)$  and, therefore, the switching points.

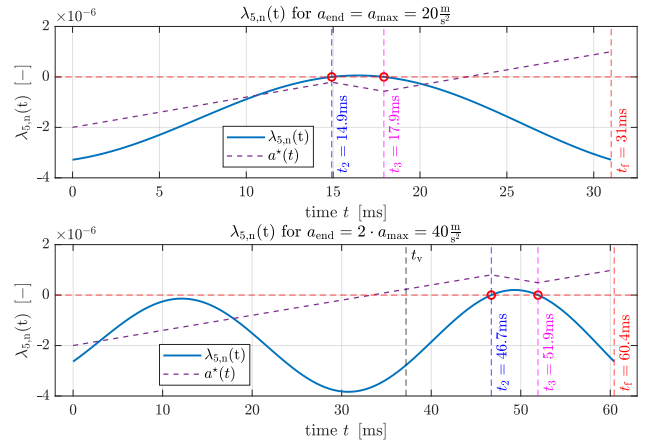


Fig. 4: Results for  $\lambda_{5,n}(t)$  for the two jerk profiles required in the trajectories shown in Figure 2. Included are the acceleration profiles  $\ddot{z}(t)$  of the jerk segments for comparison.

**Outlining the structure of the algorithm:** A graphical representation of the jerk segments can be introduced to explain the algorithm. This representation, where the jerk segments are visualized in the complex plane is introduced in Subsection IV-B. Afterwards, the calculation of the switching times is given in Subsection IV-C (developed to consider (6)). The algorithm required to compute the final time  $t_f$  (resp.

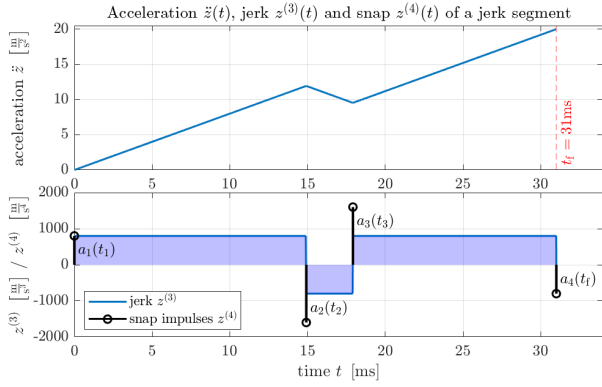


Fig. 5: Jerk segment to show the acceleration  $\ddot{z}$ , jerk  $z^{(3)}$  and coefficients  $a_1, \dots, a_4$ .

the final angle  $\varphi_f$ ) is provided after that in Subsection IV-D. Subsequently, time optimality is discussed in Subsection IV-E and the algorithm is concluded in Subsection IV-F. Since a graphical representation is used to calculate the results, most of the times are converted to angles by multiplying them with the damped angular eigenfrequency  $\omega_d$ . The plots mostly show the times however, because it is easier to read. To make the connection to the angles, the period of oscillation denoted by  $t_v$  (which corresponds to an angle of  $2\pi$ ) is marked in most plots.

### B. Introduction of graphical approach

As mentioned previously, the conditions with regards to the base displacement  $x(t)$  from (8) can be met by requiring  $\dot{x}(t_f) = 0$ . Note that, instead of the variables  $B_1$ ,  $C_1$  and  $t_f$  from (12), the switching times  $t_2, \dots, t_{n-1}$  and  $t_f$  cf. Figure 7) can be used inside the calculations directly. According to (13b) the solution of the optimal control problem corresponds to a piecewise constant jerk. This equation can be rewritten as

$$z^{(3)}(t) = \sum_{i=1}^n a_i H(t - t_i), \quad i = 1, \dots, n, \quad t_n = t_f. \quad (14)$$

with the coefficients  $a_1, \dots, a_n$  satisfying.

$$\sum_{i=1}^n a_i = 0. \quad (15)$$

For the sake of illustration, an exemplary jerk segment, obtained for  $a_{\max} = 20 \text{ m/s}^2$ , is depicted in Figure 5 to show the amplitudes  $a_1, \dots, a_4$  of the respective steps as well as the acceleration  $\ddot{z}$  and jerk  $z^{(3)}$ .

In order to determine the switching points, the trajectories  $t \mapsto \dot{x}(t)$  and  $t \mapsto \ddot{x}(t)$  associated with the internal dynamics are evaluated at  $t = t_f$ . For the piecewise constant input (14) these trajectories are given by (27a) and (27b) in Appendix B. Moreover, in view of (15), the expressions for  $\dot{x}(t_f)$  and  $\ddot{x}(t_f)$  simplify to

$$\begin{bmatrix} \dot{x}(t_f) \\ \ddot{x}(t_f) \end{bmatrix} = \mathbf{0} = \mathbf{TP}j_{\max} \begin{bmatrix} \sum_{i=1}^{n-4} a_i^* e^{\delta t_i} \cos(\omega_d t_i) \\ \sum_{i=1}^{n-4} a_i^* e^{\delta t_i} \sin(\omega_d t_i) \end{bmatrix} \quad (16)$$

with the matrices

$$\mathbf{T} = \begin{bmatrix} \frac{m_s}{k} & \frac{m_s \delta}{m_g \omega_d \omega_0^2} \\ 0 & -\frac{m_s}{m_g \omega_d} \end{bmatrix}, \quad \mathbf{P} = \begin{bmatrix} e^{-\delta t_f} \cos(\omega_d t_f) & e^{-\delta t_f} \sin(\omega_d t_f) \\ e^{-\delta t_f} \sin(\omega_d t_f) & -e^{-\delta t_f} \cos(\omega_d t_f) \end{bmatrix}.$$

Therein, dependence on  $t_f$  has been transferred to the matrix  $\mathbf{P}$ . The normalized coefficients  $a_1^*, \dots, a_n^*$  defined by  $a_i = a_i^* j_{\max}$  follow from (16) to be (cf. Figure 5 for the case  $n = 4$ )

$$a_i^* = \begin{cases} (-1)^{\nu+1}, & i = 1 \\ 2(-1)^{i+\nu}, & i = 2, \dots, n-1 \\ (-1)^{n+\nu}, & i = n \end{cases}$$

Multiplying (16) with the inverse of the regular matrix  $j_{\max} \mathbf{TP}$  from the left and introducing the complex numbers ( $i = 1, \dots, n$ )

$$s_i = a_i^* e^{\delta t_i} (\cos(\omega_d t_i) + j \sin(\omega_d t_i)) = a_i^* e^{(\delta + j\omega_d) t_i} = a_i^* e^{(p_1 + j)\varphi_i},$$

with the switching angles  $\varphi_i = \omega_d t_i$  and the normalized damping paramter  $p_1 = \frac{\delta}{\omega_d}$ , (16) can be equivalently rewritten as

$$0 = \sum_{i=1}^n a_i^* e^{(p_1 + j)\varphi_i} = \sum_{i=1}^n s_i. \quad (18)$$

For  $n = 4$  (18) is visualized in the complex plane in Figure 6. A priori, of the switching times  $t_1, \dots, t_n = t_f$ , only  $t_1 = 0$  is known. The remaining points have to be computed from the final conditions

$$a_{\max} = \sum_{i=1}^n a_i t_i \Leftrightarrow a_{\max}^* := \frac{\omega_d a_{\max}}{j_{\max}} = \sum_{i=1}^n a_i^* \varphi_i$$

in connection with (18) and the optimality condition (12).

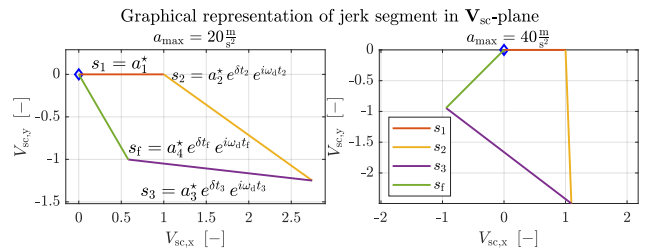


Fig. 6: Coefficients corresponding to the trajectories from Figure 4 in the complex plane.

A graphical representation of the solution from Figure 4 according to (18) is shown in Figure 6.

### C. Calculating the switching-times of the jerk segment

As seen in Figure 4 one or multiple negative segments, i.e., segments with negative jerk, might be required to reach  $a_{\max}$  in a time-optimal fashion (depending on system damping). The switching times (or switching angles) depend on the terminal time. For a given transition time  $t_f$ , the overall duration of

negative segments, called  $\Delta t_{\text{abs}}$ , can be calculated with (26a) from Appendix A and (8e) from

$$j_{\text{max}} t_f - 2j_{\text{max}} \Delta t_{\text{abs}} = a_{\text{max}}$$

to be

$$\Delta t_{\text{abs}} = \frac{j_{\text{max}} t_f - a_{\text{max}}}{2j_{\text{max}}}.$$

When using the normalized quantities, this equation simplifies to

$$\Delta \varphi_{\text{abs}} := \omega_d \Delta t_{\text{abs}} = \frac{\varphi_f - a_{\text{max}}^*}{2}. \quad (19)$$

From (19) and (13a) it follows immediately that  $\varphi_f - a_{\text{max}}^* \in [0, \pi)$  which implies

$$0 \leq \Delta \varphi_{\text{abs}} < \frac{\pi}{2}.$$

In this part of the algorithm, the switching times (resp. angles) will be computed up to a common but yet unknown shift. Those switching points are afterwards used in Subsection IV-D to compute the required shift and the corresponding switching times. In the following, three cases are distinguished, the general case with positive damping and the possibility of multiple negative jerk segments, the undamped case with  $p_1 = \delta = 0$ , and the case corresponding to one negative segment only. Naturally, the first of these cases is the most involved.

**General case:** The case, where multiple segments are required only exists, if the damping of the system is sufficiently low. To illustrate the effect, the damping has been lowered to 10% of the value from Table I for the picture shown in Figure 7. At this stage of analysis only the relative position

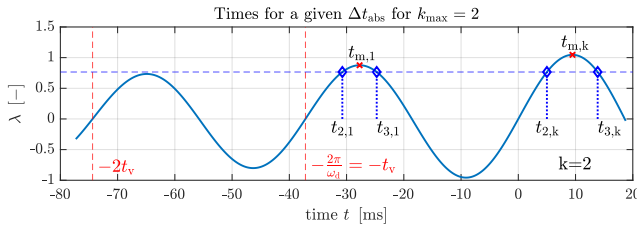


Fig. 7: Function  $t \mapsto \lambda(\omega_d t) - C_1$  with switching times.

of the switching angles w.r.t.  $\varphi_{n-1}$  is of interest:

$$\Delta \varphi_i := \varphi_{n-1} - \varphi_{2i}, \quad i = 2, \dots, n-1. \quad (20)$$

Therefore, the phase shift  $B_1$  is neglected in (12) which leads to

$$\lambda(\varphi) := \lambda_{5,n} \left( \frac{\varphi}{\omega_d} - \frac{B_1}{\omega_d} \right) = e^{p_1 \varphi} \sin(\varphi) - C_1. \quad (21)$$

In the first step, the zeros of  $\lambda$ , i.e., the relative switching angles, are computed as a function of  $C_1$ . To this end, the

local maxima of (21) are determined. Differentiating (21) with respect to  $\varphi$  gives

$$\begin{aligned} \lambda'(\varphi) &= e^{p_1 \varphi} (p_1 \sin(\varphi) + \cos(\varphi)) \\ &= e^{p_1 \varphi} \sqrt{p_1^2 + 1} \sin(\varphi + \Theta), \\ &\text{with } \Theta = \arccos\left(\frac{p_1}{\sqrt{p_1^2 + 1}}\right). \end{aligned}$$

Hence, the maxima satisfy

$$\varphi_{m,k} = (2k+1)\pi - \Theta, \quad k \in \mathbb{Z}.$$

Although not rigorously proven in this contribution, it has turned out that only the case with  $\nu = 0$  and even  $n$  is relevant, i.e., input trajectories that start and terminate with positive jerk. In this case, which solely is considered throughout the rest of the paper, it is convenient to introduce the number  $n_{\text{el}}$  of maxima (or segments with negative jerk). Obviously,  $n = 2n_{\text{el}} + 2$ .

In the considered case,  $C_1$  is always positive, as otherwise the condition (19), i.e.  $\varphi_{\text{abs}} \leq \frac{\pi}{2}$ , would be violated. Moreover,  $\lambda$  possesses two zeros in the neighbourhood of each maximum  $\varphi_{m,k}$  satisfying  $\lambda(\varphi_{m,k}) \geq 0$ . More precisely, there is a zero  $\varphi_{2k}$  on  $(\varphi_{m,k} - \pi, \varphi_{m,k})$  and a zero  $\varphi_{2k+1}$  on  $(\varphi_{m,k}, \varphi_{m,k} + \pi)$ . Having computed the maxima, the zeros  $\varphi_2, \dots, \varphi_{n-1}$  can be computed numerically since  $\lambda$  is strictly monotonic on the respective intervals. This yields a function  $\gamma$  defined by

$$\begin{aligned} \gamma(C_1, n_{\text{el}}) &= (\gamma_2(C_1, n_{\text{el}}), \dots, \gamma_{2n_{\text{el}}+1}(C_1, n_{\text{el}})) \\ &= (\varphi_2 - \varphi_{2n_{\text{el}}+1}, \dots, \varphi_{2n_{\text{el}}} - \varphi_{2n_{\text{el}}+1}, 0). \end{aligned}$$

For a given total transition time  $\varphi_f$  all relative switching angles  $n$  must be contained in the interval  $[-\varphi_f, 0]$ . Therefore,

$$n_{\text{el}} = \eta(C_1, \varphi_f) = \max\{\hat{n}_{\text{el}} \in \mathbb{N}^+ \mid \gamma_2(C_1, \hat{n}_{\text{el}}) + \varphi_f > 0\}.$$

Afterwards,  $\Delta \varphi_{\text{abs}}$  can be computed by

$$\Delta \varphi_{\text{abs}} = \rho(C_1, \eta(\varphi_f)) := \sum_{i=1}^{n_{\text{el}}} (\varphi_{2i+1} - \varphi_{2i})$$

with  $\varphi_i = \gamma_2(C_1, \eta(\varphi_f))$ . With (19), i.e.,  $\Delta \varphi_{\text{abs}} = \frac{\varphi_f - a_{\text{max}}^*}{2}$  it follows:

$$\frac{\varphi_f - a_{\text{max}}^*}{2} = \rho(C_1, \eta(\varphi_f)).$$

This latter relation can be solved for  $C_1$  for  $\varphi_f$  from the interval  $[a_{\text{max}}^*, a_{\text{max}}^* + \pi]$  which in turn delivers required relative switching angles by evaluating  $\gamma(C_1, \eta)$ . This part of the algorithm is the computationally most expensive one within the motion planning scheme. It finally provides a relation between the total transition time  $\varphi_f$  and the relative switching angles  $\varphi_2, \dots, \varphi_{2n_{\text{el}}+1}$  where the number  $n_{\text{el}}$  of negative jerk segments is another result of the algorithm. This relation is required in subsequent calculations in Subsection IV-D. Therefore, in order to allow for a fast execution, it is convenient to precompute this map once for several points from  $[a_{\text{max}}^*, a_{\text{max}}^* + \pi]$  and afterwards interpolate between those points.

**Zero damping:** If the damping equals zero, every negative segment of the solution has the same width. Therefore, the number of negative segments directly depends on the time  $t_f$  and can be calculated with

$$n_{el} = \left\lceil \frac{\omega_d t_f}{2\pi} \right\rceil = \left\lceil \frac{\varphi_f}{2\pi} \right\rceil.$$

By a symmetry argument, it follows that ( $k = 1, \dots, n_{el}$ )

$$\Delta\varphi_{2k} = 2\pi(n_{el} - k) + \frac{\Delta\varphi_{abs}}{n_{el}}, \quad \Delta\varphi_{2k+1} = 2\pi(n_{el} - k).$$

A jerk segment corresponding to  $d = 0$  is visualized in Figure 8.

**One negative jerk segment:** If there is only one negative segment, i.e.  $n_{el} = 1$ , (19) reduces to

$$\Delta\varphi_{abs} = \varphi_3 - \varphi_2 = \frac{\varphi_f - a_{max}^*}{2},$$

Hence, according to (20),

$$\Delta\varphi_2 = \varphi_3 - \varphi_2, \quad \Delta\varphi_3 = 0.$$

This case is shown on top in Figure 4 and, moreover in Figure 5.

**Graphical representation of results:** As mentioned previously all the cases are shown in Figure 8 for different values of  $\delta$ , but with the same  $t_f$  and  $\Delta t_{abs}$ . Those are only meant to show, how  $\Delta t_{abs}$  is split up between multiple negative segments (where required), relative to each other for different values of  $\delta$ . For this reason, only the constraints with respect to the slider motion governed by (8c), (8d) and (8e) are considered here. All of the curves are shifted in time axis in a way, where  $\ell_{m1}$  and  $\ell_{m2}$  are parallel, as shown in Figure 9. Actual solutions for those parameters, where all of the constraints related to base oscillation, meaning (8a) and (8b) are taken into account as well, are shown at the end of this chapter in Figure 11. The curves given here are only meant to show the influence of different damping parameters on the number of negative segments as an illustrative example. The period  $t_v$  of oscillation are also marked in the plots. Those times are slightly different since varying damping ratios lead to slightly different damped eigenfrequencies. However, these small differences are not visible with time axis scaling used. Depending on the damping, more than one negative segment might be required as visible in the plot. The calculation of the critical damping, when more than one negative segment is required is discussed in Subsection IV-E.

#### D. Algorithm to calculate the jerk segments numerically

Based on the results of the previous subsection, this section introduces the calculation required to solve the problem efficiently for any number of switching points. In order to reduce the complexity of the calculation, the problem is reduced to a line-search problem in the end with only one free variable  $\varphi_f$ . The variation of  $\varphi_f$  then leads to the solution as shown in Figure 6. The boundaries, of  $\varphi_f$  are known and given in

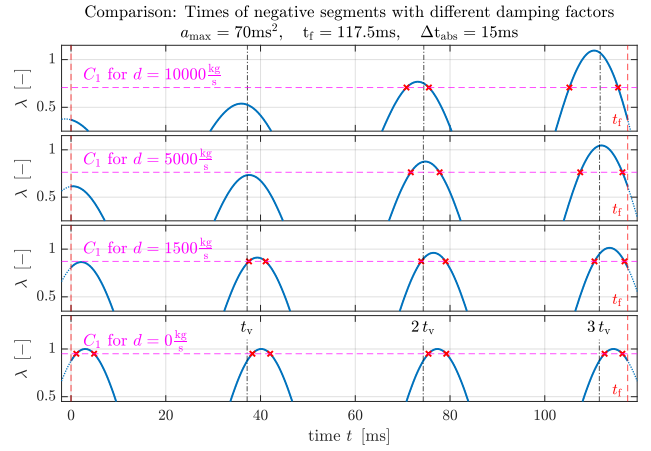


Fig. 8: Graphical representation of all cases with different values for the damping parameters, where  $t_f$  and  $\Delta t_{abs}$  coincide.

(13a). Up to a common shift, the angles  $\varphi_{2,k} = \varphi_{2k}$  and  $\varphi_{3,k} = \varphi_{2k+1}$  can be calculated directly from  $\varphi_f$ , as given by Subsection IV-C. When varying  $\varphi_f$ , the three cases shown in Figure 9 can occur. Those have been altered already to fit the

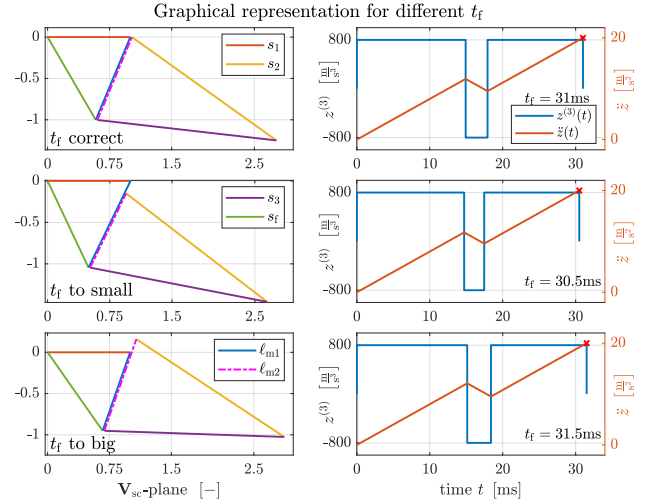


Fig. 9: Matching the absolute values of  $\ell_{m1}$  and  $\ell_{m2}$  by varying  $\varphi_f$  (respectively  $t_f$ ).

solution method explained in the following. Equation (18) can be rewritten as:

$$\underbrace{s_1 + s_n}_{\ell_{m1}(\varphi_f)} = - \underbrace{\sum_{i=2}^{n-1} s_i}_{\ell_{m2}(\varphi_f, \varphi_f)}, \quad s_i = a_i^* e^{(p_1+j)\varphi_i} \quad (23)$$

The left hand side of this equation spans a triangle in the complex plane while the right hand side corresponds to a polygon with  $n-1$  edges (cf. Figure 9 for  $n = 4$  and Figure 12 for  $n \in \{4, 6, 8\}$ ).

Now observe, that for a chosen sequence of coefficients, i.e., given parameters  $\nu$  and  $n$ , the left hand side of (23) is

completely determined by  $\varphi_f$ , i.e.,

$$\ell_{m1}(\varphi_f) = s_1 + s_n = a_1^* + a_n^* e^{(p_1+j)\varphi_f}.$$

Moreover, as

$$\varphi_i = \varphi_{n-1} - \Delta\varphi_i, \quad i = 2, \dots, n-1 \quad (24)$$

where, according to Subsection IV-C  $\Delta\varphi_i$  is determined by  $\varphi_f$ , the right hand side of (23) can be rewritten in the form

$$\ell_{m2}(\varphi_f, \varphi_{n-1}) = - \sum_{i=2}^{n-1} s_i = e^{(p_1+j)\varphi_{n-1}} \bar{\ell}_{m2}(\varphi_f)$$

with

$$\bar{\ell}_{m2}(\varphi_f) = - \sum_{i=2}^{n-1} a_i^* e^{-(p_1+j)\Delta\varphi_i}.$$

As a consequence, (23) appears in the form

$$\ell_{m1}(\varphi_f) = e^{(p_1+j)\varphi_{n-1}} \bar{\ell}_{m2}(\varphi_f).$$

The argument of the right hand side can be matched to that of the left hand side by computing

$$\bar{\psi}(\varphi_f) = \arg(\ell_{m1}(\varphi_f)) - \arg(\bar{\ell}_{m2}(\varphi_f))$$

and choosing

$$\varphi_{n-1} = \psi(\varphi_f) = \bar{\psi}(\varphi_f) + 2\pi \left\lfloor \frac{\varphi_f - \bar{\psi}(\varphi_f)}{2\pi} \right\rfloor. \quad (25)$$

As the argument of a complex number is defined only up to a multiple of  $2\pi$ , the latter correction is required to comply with the switching law (6) in view of the periodic switching function (12). This ensures that the final switching occurs at the zero of (12) closest to  $\varphi_f$ .

Having matched the arguments of  $\ell_{m1}$  and  $\ell_{m2}$ , the problem is reduced to the computation of the zeros of

$$\bar{\ell}(\varphi_f) := |\ell_{m1}(\varphi_f)|^2 - \left| e^{(p_1+j)\psi(\varphi_f)} \bar{\ell}_{m2}(\varphi_f) \right|^2.$$

This is achieved numerically by a line search on the interval  $[a_{\max}^*, a_{\max}^* + \pi]$  (cf. (13a)).

The errors  $\varphi_f \mapsto \bar{\ell}(\varphi_f)$  for different maximal accelerations  $a_{\max}$  are shown on the entire intervals (13a) in Figure 10. The jerk segments corresponding to the trajectories in Figure 4 are marked by the solid lines. After  $\varphi_f$  is calculated, the angle

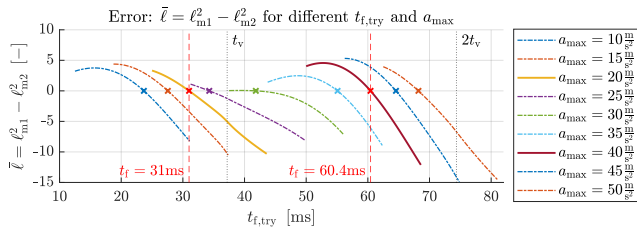


Fig. 10: Showing  $\bar{\ell}$  and the final  $t_f$  for jerk segments of different acceleration.

$\varphi_{n-1}$  can be computed directly by using (25) which in turn delivers  $\varphi_2, \dots, \varphi_{n-2}$  by (24). The switching times follow immediately from the switching angles via  $t_i = \frac{\varphi_i}{\omega_d}$ .

## E. Discussion of time-optimality of jerk segments

**Full jerk segments as calculated with the algorithm:** The presented algorithm is applied to the same parameters that were used in Figure 8 to show the computed jerk segments that satisfy all the constraints provided by (4) and (5). The corresponding trajectories are shown in Figure 11. The required

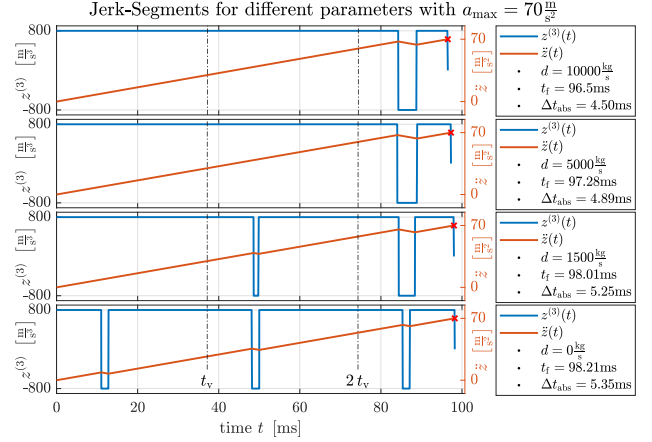


Fig. 11: Actual jerk segments for the same parameters as provided by Figure 8.

values for  $\Delta t_{\text{abs}}$  are given and the resulting  $t_f$  as well. The representation of those jerk segments in the complex plane is shown in Figure 12. All of those jerk segments comply with

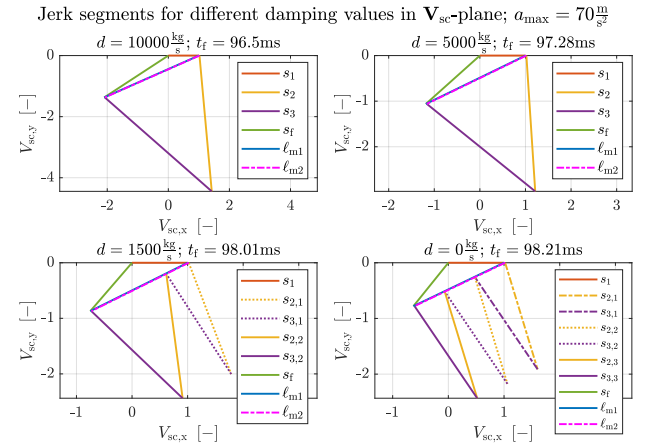


Fig. 12: Actual jerk segments for the same parameters as provided by Figure 8. Trajectories from Figure 11 represented in the complex plane. Effect on damping best visible when comparing the length's of  $s_1$  with  $s_f$ .

the necessary conditions for a local optimum as outlined by the PMP. Since, this is the only possible solution that allows to satisfy the constraints (8) while complying with the switching law for the input (6), it can be concluded, that this is in fact the globally best solution for the problem defined.

**Analysis of critical damping:** This section continues with further analysis regarding the number of segments and its connection to time optimality. As shown in Figure 8, depending



on the damping of the system, multiple negative segments might be required to ensure optimality of the jerk segments. An analysis is shown in Figure 13 to calculate the critical damping for different  $a_{\max}$  values. This critical damping is the magnitude of the damping parameter, where more than one negative jerk segments is required (if the damping is below this critical value). To obtain the critical damping, starting from

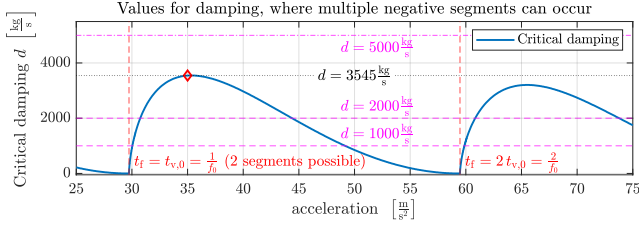


Fig. 13: Values for damping, when multiple segments are required. Compared to the damping from Table II, the damping where multiple negative segments can actually occur is lower.

an initial value, the damping has been decreased until more than one negative segment was required for the computation of the jerk segments. This procedure has been performed for different values of  $a_{\max}$ . If the critical damping is smaller than the damping given, which is the case for the parameters in Table I, the solution with one negative segment is the time-optimal solution for the jerk segments. It can be seen, that the critical damping depends on the maximal acceleration  $a_{\max}$  (also compare the jerk segment for  $a_{\max} = 29 \text{ m/s}^2$  and  $a_{\max} = 36 \text{ m/s}^2$  in Figure 15). However, even if the optimal solution requires more than one negative segment, there are trajectories with only one negative segment which comply with the terminal constraints. Moreover, the numerical results presented in Figure 14 show, that the actual time advantage of using multiple negative segments is small, if not negligible. The time advantage of taking multiple negative segments into

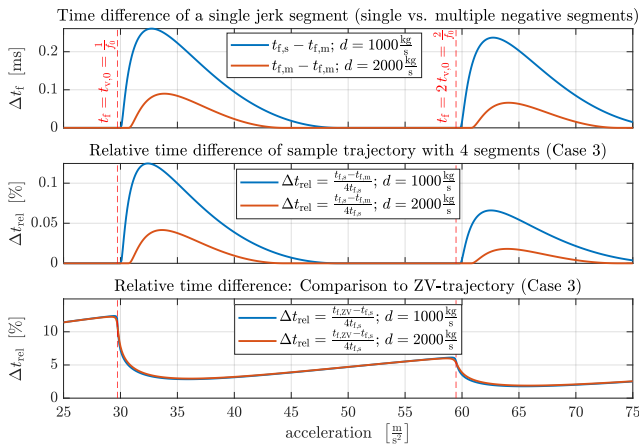


Fig. 14: Actual time-advantage of segments, when using more than one negative segment Figure 8

account is as low as 0.1%. In contrast, the time advantage of the OCP-J (cf. [3]) approach compared to a ZV-shaped S-Curve

can be as high as 10%. The damping used for comparison is not the one from Table I, as this set of parameters requires exactly one negative segment, regardless of the maximal acceleration. For this reason, the damping parameter marked in Figure 13 has been used for this comparison, since it may cause multiple negative segments.

### F. Edge-case

With the algorithm presented in this section, the jerk segments required to assemble the trajectory (as demonstrated in [3]) can be calculated. The optimal control problem is formulated in a way, that  $a_{\max}$  is reached at the terminal time  $t_f$  of the jerk segment. Since the acceleration is unconstrained on  $t \in (0, t_f)$ ,  $\ddot{z}(t)$  can be higher than  $\ddot{z}(t_f)$ , as shown in Figure 15. This happens only on a small interval and, as

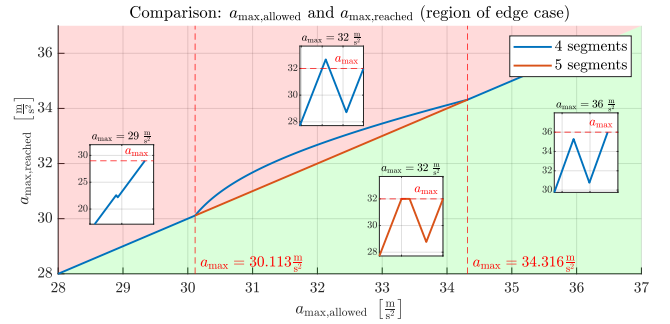


Fig. 15: Showing, the maximum acceleration on  $t \in [0, t_f]$  and showing the interval, where the edge case can occur.

Figure 6 and Figure 4 show, it does not come into effect for  $a_{\max} = 2 \cdot a_{\text{lim}}$  (required for the trajectory shown on the left in Figure 2) for the parameters used in this publication. Introducing another 5<sup>th</sup> step into the jerk segment (with this a section with  $j(t) = 0$ ) can help to remedy this issue as shown in Figure 15. Implementation into the algorithm, further analysis when it appears and implementation details of the required calculation is scope for planned future work.

## V. CONCLUSION AND OUTLOOK

An efficient algorithm was introduced to calculate the jerk segments. According to [3], quick recomputation of the jerk segments may be required to ensure minimal transition times  $t_{t,t}$  for trajectories composed of several motion primitives and the algorithm presented here achieves exactly that. The calculation further does not rely on complex numerical optimization procedures or algorithms, which enables implementation on PLC's with limited computation power. The most important next step is an implementation on a PLC to utilize the algorithm presented here for the trajectory-planning method introduced in [3] to test the computation times on actual hardware. Adapting the algorithm to only allow switches of jerk on full controller cycles will be studied in the future as well in combination with active control algorithms on a production machine. Possible extensions of the algorithm to take multiple eigenfrequencies into account may pave the way for the application to systems with multiple elastic

modes. Moreover, extension to rest-to-rest transitions of the full system dynamics, called OCP-S in [3], might offer even faster transition times. Another conceivable application of the jerk segments as motion primitives would be in a graph-based trajectory planning algorithms, such as rapidly exploring random trees [17], to plan trajectories in multi-dimensional configuration spaces.

## REFERENCES

- [1] Jonathan Abdilla, Uwe Bayer, Ruurd Boomsma, Stephan Bulcher, Alexander Kalss, Stephan Martin, Harald Meixner, Thiago Moura, Hubert Selhofer, Wolfgang Voegelé, and Martin Widauer. Thermo compression bonding for large dies under protective atmosphere. In *2020 IEEE 70th Electronic Components and Technology Conference (ECTC)*. IEEE, jun 2020.
- [2] Michael Athans and Peter L. Falb. *Optimal control - An Introduction to the Theory and Its Applications*. Dover Publ., Mineola, New York, 2007.
- [3] Thomas Auer and Frank Woittennek. Computationally efficient trajectory design from motion primitives for near time-optimal transitions for systems with oscillating internal dynamics. *preprint*, 2024.
- [4] Thomas Auer and Frank Woittennek. On trajectory design for flexible structures with input and state constraints. *IFAC*, 2023.
- [5] Thomas Auer and Frank Woittennek. On improving the settling time for highly-accurate pick-and-place processes with experimental validation. In *2024 IEEE 20th International Conference on Automation Science and Engineering (CASE)*, pages 3683–3690. IEEE, August 2024.
- [6] Lars Berscheid and Torsten Kroeger. Jerk-limited real-time trajectory generation with arbitrary target states. In *Robotics: Science and Systems XVII*. Robotics: Science and Systems Foundation, jul 2021.
- [7] Marius Beul and Sven Behnke. Analytical time-optimal trajectory generation and control for multirotors. In *2016 International Conference on Unmanned Aircraft Systems (ICUAS)*. IEEE, jun 2016.
- [8] Xiaohua Cao, Chao Meng, Yong Zhou, and Meng Zhu. An improved negative zero vibration anti-swing control strategy for grab ship unloader based on elastic wire rope model. *Mechanics and Industry*, 22:45, 2021.
- [9] B.G. Dijkstra, N.J. Rambaratsingh, C. Scherer, O.H. Bosgra, M. Steinbuch, and S. Kerssemakers. Input design for optimal discrete time point-to-point motion of an industrial xy-positioning table. In *Proceedings of the 39th IEEE Conference on Decision and Control (Cat. No.00CH37187)*, CDC-00. IEEE, 2007.
- [10] A. Feldbaum. Optimal processes in systems of automatic control. *Avtomatika i Telemekhanika* 14.6, 1953.
- [11] R. Haschke, E. Weitnauer, and H. Ritter. On-line planning of time-optimal, jerk-limited trajectories. In *2008 IEEE/RSJ International Conference on Intelligent Robots and Systems*. IEEE, September 2008.
- [12] Leslie M. Hocking. *Optimal Control - An Introduction to the Theory with Applications*. Oxford University PressOxford, February 1991.
- [13] Chul-Goo Kang. Impulse vectors for input-shaping control: A mathematical tool to design and analyze input shapers. *IEEE Control Systems*, 39(4):40–55, aug 2019.
- [14] Mateusz Kasprowiak, Arkadiusz Parus, and Marcin Hoffmann. Vibration suppression with use of input shaping control in machining. *Sensors*, 22(6):2186, mar 2022.
- [15] Joonyoung Kim and Elizabeth A. Croft. Preshaping input trajectories of industrial robots for vibration suppression. *Robotics and Computer-Integrated Manufacturing*, 54:35–44, December 2018.
- [16] Phillip Kronthaler. *Optimization of Handling Processes by Means of Model-Based Control Engineering*. PhD thesis, UMIT TIROL GmbH, 2022.
- [17] Steven Michael LaValle. *Planning Algorithms*. Cambridge University Press, Cambridge, 2009.
- [18] Wilson Linda S., Balestra Francis, Sangiorgi Enrico, Hayashi Yoshihiro, Takaura Norikatsu, Ishiuchi Hidemi, Gargini Paolo, and Conte Tom. International Roadmap for Devices and Systems (IRDS). Technical report, IEEE, 2023.
- [19] Mohammad Javad Maghsoudi, Z. Mohamed, S. Sudin, S. Buyamin, H.I. Jaafar, and S.M. Ahmad. An improved input shaping design for an efficient sway control of a nonlinear 3d overhead crane with friction. *Mechanical Systems and Signal Processing*, 92:364–378, August 2017.
- [20] P.H. Meckl and P.B. Arestides. Optimized s-curve motion profiles for minimum residual vibration. In *Proceedings of the 1998 American Control Conference. ACC (IEEE Cat. No.98CH36207)*. IEEE, 1998.
- [21] Lucy Y. Pao and William E. Singhose. Robust minimum time control of flexible structures. *Automatica*, 34(2):229–236, feb 1998.
- [22] Quang-Cuong Pham. A general, fast, and robust implementation of the time-optimal path parameterization algorithm. *IEEE Transactions on Robotics*, 30(6):1533–1540, December 2014.
- [23] L.S. Pontrjagin, V.G. Boltjanskij, R.V. Gamkrelidze, and E.F. Misčenko. *Mathematische Theorie Optimaler Prozesse*. München / Wien, R.Oldenbourg Vlg., 1964.
- [24] N. Singer, W. Singhose, and W. Seering. Comparison of filtering methods for reducing residual vibration. *European Journal of Control*, 5(2-4):208–218, jan 1999.
- [25] Neil C Singer. *Residual vibration reduction in computer controlled machines*. Massachusetts Institute of Technology, 1989.
- [26] W. Singhose, W. Seering, and N. Singer. Residual vibration reduction using vector diagrams to generate shaped inputs. *Journal of Mechanical Design*, 116(2):654–659, June 1994.
- [27] W. E. Singhose, L. J. Porter, T. D. Tuttle, and N. C. Singer. Vibration reduction using multi-hump input shapers. *Journal of Dynamic Systems, Measurement, and Control*, 119(2):320–326, jun 1997.
- [28] W.E. Singhose, W.P. Seering, and N.C. Singer. Shaping inputs to reduce vibration: a vector diagram approach. In *Proceedings., IEEE International Conference on Robotics and Automation*. IEEE Comput. Soc. Press, 1990.
- [29] W.E. Singhose, Neil Singer, Convolv Inc, and Warren Seering. Design and implementation of time-optimal negative input shapers. March 1996.
- [30] Khalid L. Sorensen, Aayush Daftari, William E. Singhose, and Keith Hekman. Negative input shaping: Eliminating overcurrenting and maximizing the command space. *Journal of Dynamic Systems, Measurement, and Control*, 130(6), oct 2008.
- [31] Joshua Vaughan, Aika Yano, and William Singhose. Comparison of robust input shapers. *Journal of Sound and Vibration*, 315(4-5):797–815, sep 2008.
- [32] Yunan Wang, Chuxiong Hu, Zeyang Li, Shize Lin, Suqin He, and Yu Zhu. Time-optimal control for high-order chain-of-integrators systems with full state constraints and arbitrary terminal states. *IEEE Transactions on Automatic Control*, pages 1–16, 2024.
- [33] Yong Zhou, Xinyuan Zhang, Zhenzhen Yu, Dingena Schott, and Gabriel Lodewijks. An improved zero vibration method and parameter sensitivity analysis for the swing control of bridge-type grab ship unloader. *Proceedings of the Institution of Mechanical Engineers, Part C: Journal of Mechanical Engineering Science*, 230(14):2463–2472, July 2015.

## APPENDIX A

### SLIDER MOVEMENT FOR PIECEWISE CONSTANT JERK $z^{(3)}$

Trajectories of the form (14) with  $n$  jumps in the jerk  $z^{(3)}(t)$  of amplitudes  $a_1, \dots, a_n$  occurring at  $t_1 < \dots < t_n$  are considered. The acceleration (26a), velocity (26b) and position (26c) can be calculated by integrating and taking the initial conditions values into account. This leads to

$$\ddot{z}(t) = \ddot{z}_0 + \sum_{i=1}^n a_i \cdot (t - t_i), \quad (26a)$$

$$\dot{z}(t) = \dot{z}_0 + \ddot{z}_0 t + \frac{1}{2} \sum_{i=1}^n a_i \cdot (t - t_i)^2, \quad (26b)$$

$$z(t) = z_0 + \dot{z}_0 t + \ddot{z}_0 \frac{t^2}{2} + \frac{1}{6} \sum_{i=1}^n a_i \cdot (t - t_i)^3 \quad (26c)$$

with  $\ddot{z}_0$ ,  $\dot{z}_0$  and  $z_0$  being the initial values.

## APPENDIX B

### BASE MOVEMENT FOR PIECEWISE CONSTANT JERK $z^{(3)}$

Generally, trajectories with jumps in the jerk  $z^{(3)}(t)$ , as given in Appendix A, are analysed. The calculations shown here all show the result for the base motion  $x$ ,  $\dot{x}$ ,  $\ddot{x}$  and  $x^{(3)}$  to an impulse in the snap  $z^{(4)}$  with length  $a_i$ . The damping  $\delta$  of the system and the damped angular frequency  $\omega_d$  are calculated with

$$\delta = \frac{d}{2m_g}, \quad \omega_0^2 = \frac{k}{m_g}, \quad \omega_d = \sqrt{\omega_0^2 - \delta^2}.$$

Assuming, that  $x_0$  and all its derivatives vanish at  $t = 0$ , taking multiple impulses in  $z^{(4)}$  into account (see (14)) and using  $\tau_i = t - t_i$ , gives the symbolic solution for the base motion

$$\ddot{x}(t) = \sum_{i=1}^n -a_i \frac{m_s}{m_g \omega_d} e^{-\delta \tau_i} \sin(\omega_d \tau_i) \cdot H(\tau_i), \quad (27a)$$

$$\dot{x}(t) = \sum_{i=1}^n a_i \frac{m_s}{m_g \omega_d \omega_0^2} \left[ e^{-\delta \tau_i} \cdot (\omega_d \cos(\omega_d \tau_i) + \delta \sin(\omega_d \tau_i)) - \omega_d \right] \cdot H(\tau_i), \quad (27b)$$

$$x(t) = \sum_{i=1}^n a_i \frac{m_s}{m_g \omega_d \omega_0^4} \left[ e^{-\delta \tau_i} \cdot \left( (\omega_d^2 - \delta^2) \sin(\omega_d \tau_i) - 2\omega_d \delta \cos(\omega_d \tau_i) \right) - \omega_d \omega_0^2 \tau_i + 2\delta \omega_d \right] H(\tau_i). \quad (27c)$$

The base velocity (27b) and base position (27c) are calculated via integration from the acceleration (27a). Deriving (27a) with respect to the time gives the jerk of the base

$$x^{(3)}(t) = \sum_{i=1}^n -a_i \frac{m_s}{m_g \omega_d} \left[ e^{-\delta \tau_i} \cdot (\omega_d \cos(\omega_d \tau_i) + \delta \sin(\omega_d \tau_i)) \right] \cdot H(\tau_i).$$